A function-driven characterization of printed conductors on PV cells

A function-driven characterization of printed conductors on PV cells

Roberto Bellotti[1], Valentina Furin[2], Claire Maras[3], Gian Bartolo Picotto[1], Luigi Ribotta[1]*

[1]Istituto Nazionale di Ricerca Metrologica (INRIM), Strada delle Cacce 91, 10135, Torino, Italy

[2]Applied Materials Italia s.r.l. (AMAT), via Postumia Ovest 244, 31048, Treviso, Italy

[3]EPF – École d'ingénieur-e-s, 3 bis Rue Lakanal, 92330, Sceaux, France

*Corresponding author: l.ribotta@inrim.it

Keywords: printed conductors, morphology, resistance, uncertainty, material measure

Abstract

Nowadays the development in PV cells manufacturing requires increasingly sophisticated technologies, and in order to avoid efficiency losses in PV cell, printing techniques of the front contacts have to be well controlled. To this purpose, printed linear conductors (PLCs) on a PV standard cell are characterized by morphology- and resistance-based measurements, creating a well-calibrated test structure towards the development of an application-oriented material measure. It can be noticed that morphology and texture parameters determined by stylus and optical profilers are well in agreement, and the resistance calculated from the reconstructed cross-section area matches quite well the measured resistance of fingers. Uncertainties of about 14 % to 17 % are estimated for local measurements of morphology-based and measured resistance of finger segments up to 5 mm length. Fingers characterized by somewhat larger roughness/waviness values (Ra, Rq, Wt) show some local irregularities, which may degrade the electrical contact of the PV front surface.

1. Introduction

Nowadays the manufacturing of front contact in photovoltaic (PV) cells requires silver paste which can be deposited with screen printed techniques [1]. These contacts, which allow the electrical connection between the semiconductor front surface, should have a good design and fabrication in order not to decrease solar cell efficiency [2]. To verify the functional performance, surface topography parameters and sizes of fingers, i.e., roughness, height and cross-section area [3], are studied in this work; furthermore, related to topographic measurements, resistance measurements are performed. Fingers are measured locally on selected sampling areas with the aim of creating a test structure with well calibrated morphology parameters and line resistance of fingers towards the development of an application-oriented reference sample [4], suitable to reproduce morphology and electrical quantities to support traceability of in-line and off-line quality controls in PV cell production. Future steps will concern a study of the overall stability of the given quantities during the use of such test structures.

2. Test structure

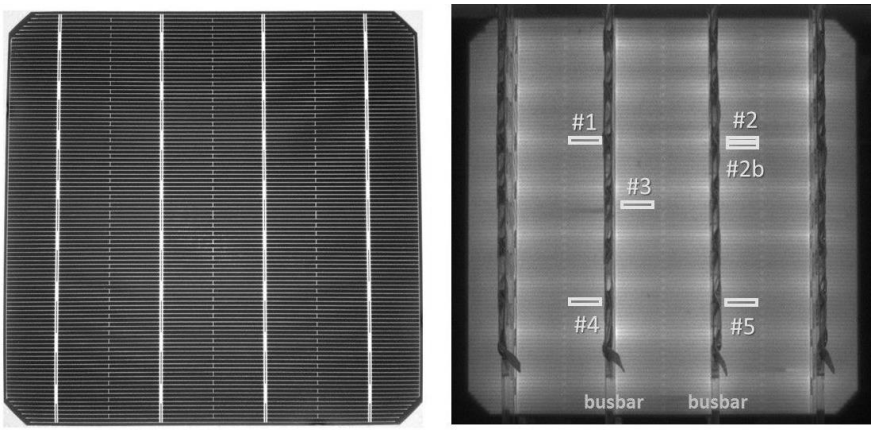

Figure 1 Photograph (left) and electroluminescence (EL) image (right) of the PV cell; sampling areas are highlighted as white boxes in the EL image

AMAT (Applied Materials) prints fingers on crystalline silicon (c-Si) PV cells using PLC technique. These electric contacts, obtained from a Heraeus 9642B paste, are undergone to a curing temperature of 820 °C for about 3 seconds, in order to create the contact between the c-Si and the fingers. In Figure 1 are shown the cell, whose dimensions are of 156 mm x 156 mm x 0.18 mm, made by 101 fingers and 4 busbars, and its electroluminescence (EL) image, which is taken with an IR camera by fixing voltage and varying the current through the cell. In the EL image are highlighted six areas, most of them flawless, which were extensively analyzed performing both topographic and resistance measurements. The six areas selected do not show evident variations of light contrast in the EL image and are expected to be free from interruptions of the printed lines (fingers).

3. Experimental measurements

3.1 Instrumentation and setup

Morphological measurements are performed by using tactile and optical methods, more specifically stylus and optical confocal instruments. Stylus-based profilers are widely used for 2D roughness measurements with a lateral resolution driven by the tip size/shape and sampling interval, while a nanometer level resolution is achieved with the vertical axis of the instrument. Optical profilers operating with interferometric and confocal heads may provide a sub-nanometer vertical resolution and a lateral resolution driven by the pixel size and limited by diffraction at the highest magnification. Edges effects due to tactile tip geometry and to the numerical aperture of the optical objectives are present in both techniques, namely with steep slopes or high-aspect ratio surface structures. Furthermore, tactile instruments suffer from a relatively slow scanning rate, while non-contact instruments overcome such a limitation, but other limitations may come due to imaging artefacts with local variations of the optical properties of surfaces [5].

The stylus profiler in use is a Taylor Hobson Form TalySurf Series 2, with a 2.5 µm nominal radius tungsten tip. The z-movement of the stylus tip is read by an interferometer head, while the form/waviness/roughness of the specimen is sampled (Figure 2). Besides of the lateral movement (x-axis) provided by the stylus head, a 3D profiling is achieved by moving the sample along the y-axis with a motorized stage offering 1 µm step resolution [6]. The stylus tip in contact with the surface of a finger measures a 2D profile at each scan line, while a 3D reconstruction is achieved by all these profiles from several parallel scan lines, equally spaced of 10 µm, each of them made by 10000 data points.

The stylus instrument is calibrated by a precision ceramic ball, which in turn is calibrated (mean diameter) by an interferometric setup. As recommended by the manufacturer (Taylor-Hobson) the stylus pick-up traverses the top profile of a spherical cap of the precision ball to determine the z-sensitivity and Pt parameter, that is the total height of the primary profile [6]. The lower the Pt value the better the geometry of the tip apex. The lateral scale of the instruments is calibrated by a precision photomask with parallel chromium (Cr) lines forming a periodical structure up to tens of millimeter size.

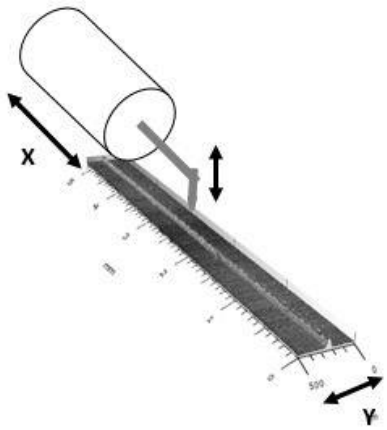

Figure 2 Sketch of stylus and sample movements for 3D tactile profiling.

The optical profiler in use is a Sensofar PLμ 2300, which lies on a Halcyonics Micro 60 antivibration table, this last placed on an optical table with laminar flow isolator supports. The instrument provides optical images of 768 x 576 pixels, which represent a surface area of about 257 μm x 191 μm with a X50 objective. By the own-instrument driving software (SensoScan) finger length up to several millimeters are recorded at high resolution by the image stitching, i.e., a long rectangular area of about 5 mm x 0.2 mm is made by stitching 25 images along the finger line. Topographic measurements are performed in intensity confocal mode, an imaging method for areal and profile surface measurements for a wide range of textures from smooth to rough surfaces. Confocal imaging sets itself apart from standard light microscopy through the use of confocal apertures, that ensure only light at the point of focus on the test surface enters the detector. To build up a 3D image the sample is vertically scanned creating multiple optical sections along the z direction, such that each point on the sample surface passes through the focal plane of the microscope. The signal collected at a single point on the object during a vertical scan is evaluated for maximum irradiance, which corresponds to the imaged point being in focus [7,8]. An interferometer set-up is used for in-situ calibration of the vertical axis of the optical profiler operating either with a phase-grating displacement transducer coupled to the vertical axis or with a piezo-resistive sensor inside the objective moving stage. Suitable artefacts based on 2D gratings calibrated by an optical diffractometer are used to determine the magnification (pixel size) of objectives.

3D images recorded either by optical and stylus profilers are then analyzed by metrological software tools [9,10], by which quantitative values of morphology parameters (thickness, width, slope and top roughness) of fingers are calculated and compared.

Resistance measurements make use of an Agilent Keysight 3458A multimeter, operating with a 4-wire like resistance setup (Figure 3). A reference electrode provides the electrical contact to a busbar and by separate wires to the Low Sense and Low Input of the multimeter, while a working electrode provides the electrical contact to the measuring position along the finger segment and by separate wires connected to the Hi Sense and Hi Input. Both electrodes use elastic and retractable tips with a slightly rounded apex, by which a good contact with fingers is achieved. At contact, the tip is loaded of about 0.15 N. The calculated elastic deformation at contact is of about 45 nm [11].

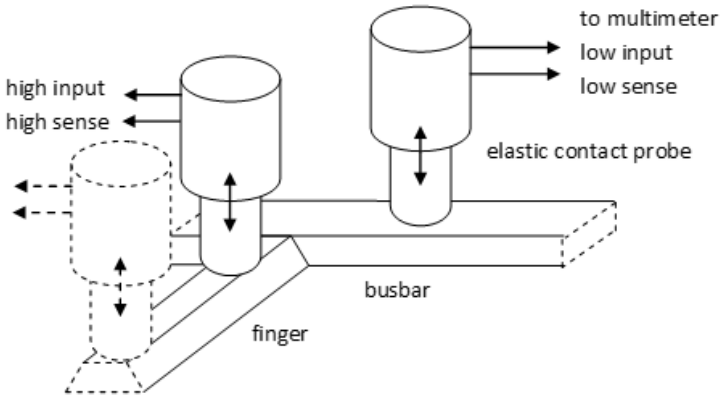

Figure 3 Sketch of the 4-wire like set-up used for resistance measurements. Contact probes, finger and busbar are not to scale.

3.2 Measurement runs

Optical and tactile imaging are made on selected areas of the PV cell as shown in Figure 1. Fingers are imaged around their mid length for a segment about 5 mm long. Then, resistance measurements are performed on the same segments of finger for comparison.

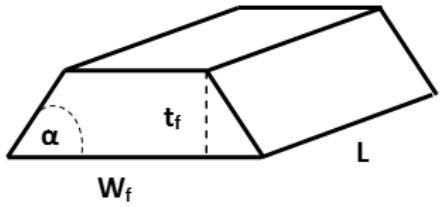

Figure 4 Assumed shape and parameters of a finger

The fingers are approximated as polyhedrons (Figure 4) with a trapezoidal cross-section area, according to a work by Jiang et al. [12]. The cross-section area *A* is given by the equation (1), where W_f is the base width of the trapezium, t_f is the height, α is the angle of the finger sidewall to the horizontal and L is the length of the finger segment.

$$A = \left(W_f - \frac{t_f}{\tan\alpha}\right) \cdot t_f \qquad (1)$$

Resistance measurements are related to morphological measurements according to the equation (2), where ρ_f is the finger resistivity, equal to 2.7×10^{-6} Ω·cm for silver paste [12], and d_l is the elementary segment length.

$$Rcs_i = \frac{\rho_f}{A_i} \cdot d_l \qquad (2)$$

The cross-section area-based calculated resistance $Rcs = \sum_{i=1}^{n} Rcs_i$, is obtained by the sum of the elementary Rcs_i up to r the given length l of the finger segment. Therefore, it takes into account all the local variations of the finger cross-section area, e.g., variations here represented by valleys and peaks of a "profile" of the cross-section area Acs along the segment. Such a "profile" describes a 3D-like roughness of the finger [13].

4. Results

4.1 Topographic measurements

Measurements were taken with optical and stylus profilers at the five sampling areas as highlighted in the Figure 1 of the cell. Reconstructed surfaces are of 5 mm x 190 µm for optical stitched images (objective X50), while for stylus topographies are of 5 mm x 500 µm (Figure 5).

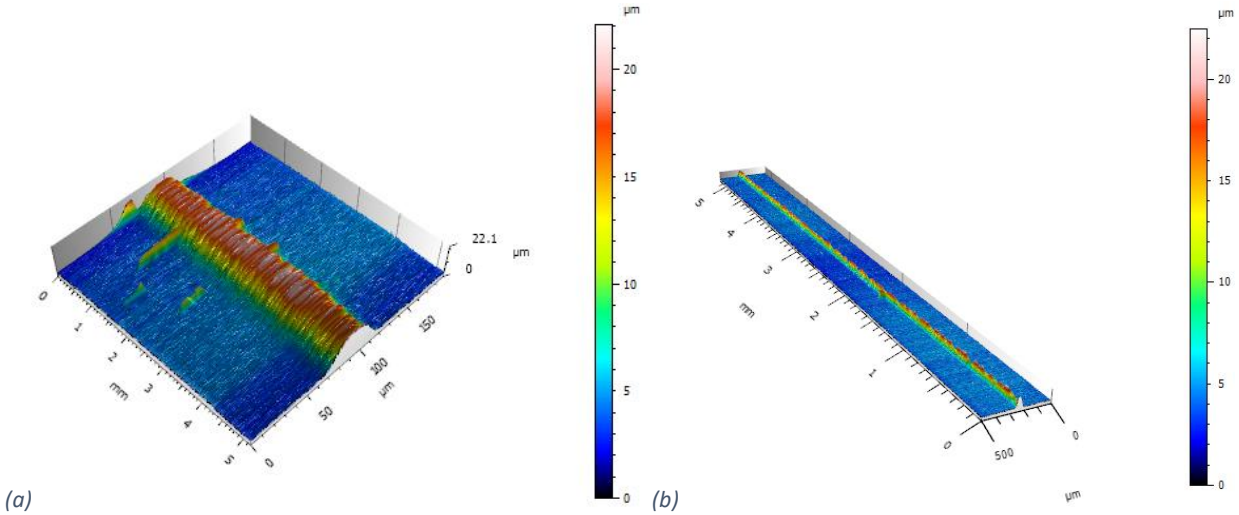

Figure 5 Optical (a) and stylus (b) topographies of the finger at position #5

The cross-section area (Acs, mean and rms values) and the wavelength of the dominant components of the Acs determined by metrological tools [9,10], are given in Table 1 for all sampled areas/instruments and are plotted in the Figures 6 and 7 for the area #5 of the cell.

Table 1 Mean value and other parameters calculated from the cross-section area (Acs) of fingers, as reconstructed by optical confocal (opt) and stylus (st) instruments along the finger segment.

sampling areas	**#1**		**#2**		**#2b**		**#3**		**#4**		**#5**	
finger evaluation length of 5 mm	*opt*	*st*	*opt*	*st*	*opt*	*st*	*opt*	*st*	*opt*	*st*	*opt*	*st*
wavelength of the main components of *Acs* [µm]	~ (100 – 200)											
mean cross-section area Acs [µm^2]	392	377	392	413	385	375	407	371	413	398	388	379
rms (Acs) [µm^2]	114	99	165	147	80	77	79	74	66	62	84	75
cross-section area-based calculated resistance Rcs [mΩ]	440.0	416.1	636.7	736.8	382.6	401.7	357.1	402.9	347.0	375.4	396.9	403.2
st. dev. of residuals by a linear fit of Rcs[mΩ]	0.14	0.02	0.37	0.73	0.02	0.01	0.01	0.01	0.06	0.01	0.06	0.35

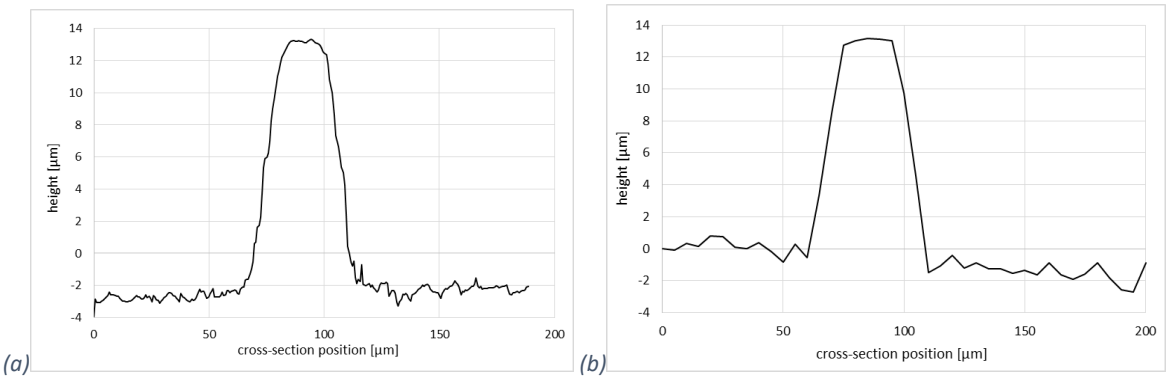

Figure 6 Area #5: finger cross-section area obtained by means of (a) optical and (b) stylus profilers

Figure 6 shows the trapezoidal shape of the cross-section of the finger, as reconstructed by optical and stylus instruments. It can be observed that the two plots agree quite well in finger shape and sizes, and therefore the optical and stylus reconstructions look robust and validated by each other. The plot obtained by confocal imaging shows more details compared to the other by stylus because of a better spatial resolution.

Besides of the mean and rms values of the cross-section area, in Table 1 are given the calculated resistance Rcs (formula (2)) together with the standard deviation of residuals by a linear fit of Rcs. This last highlights the presence of significant morphology variations of the finger segment.

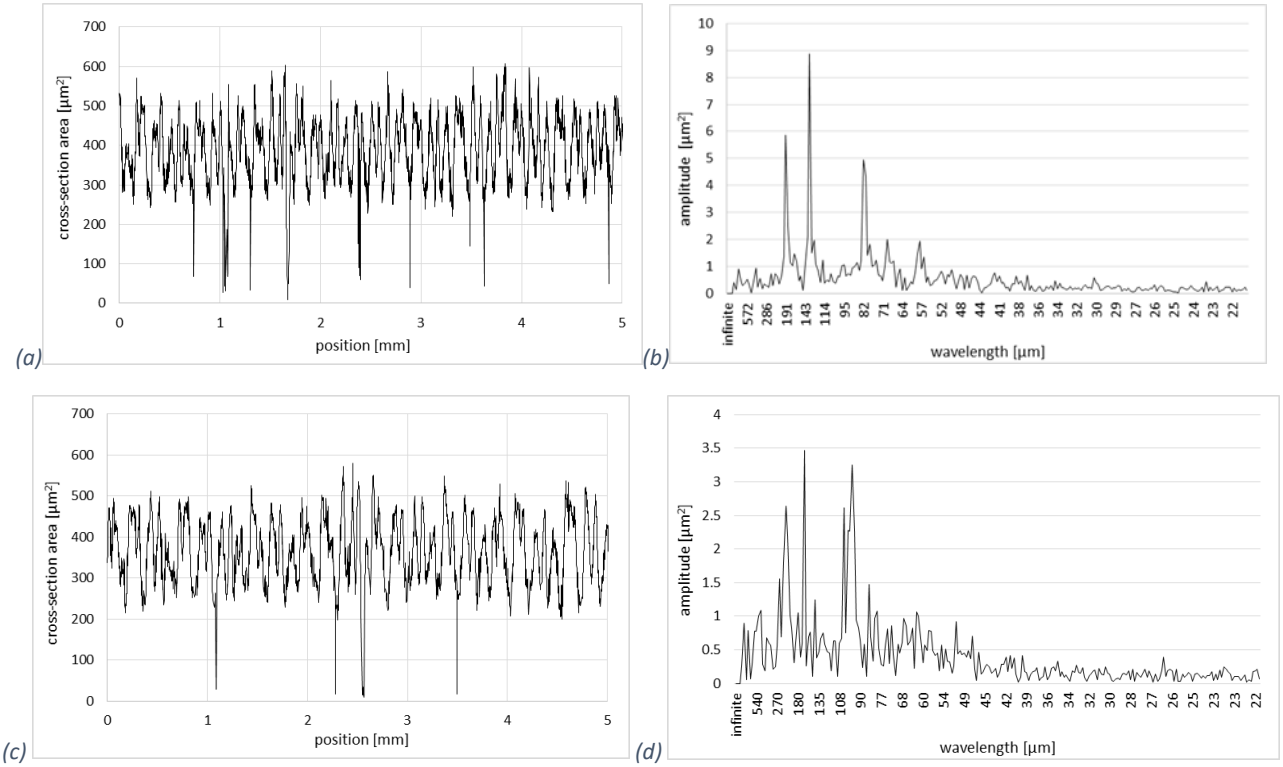

Figure 7 Area #5: Profile of cross-section area variations and its spatial frequency spectrum calculated by (a),(b) optical- and (c),(d) stylus- based images-

The profile of the cross-section area variation along the finger segment are shown in Figure 7 together with associated spatial frequency spectrum [9,10]. It is worth noting that optical- and stylus-based profiles differs by the number of "spikes" and by their positions along the finger segment. Mostly like valleys of the finger cross-section, these spikes draw somewhat large restrictions of the cross-section, thus influencing the local finger resistance. Confocal-based images may suffer from void pixels and artefacts due to local

variations of optical surface properties but provide a lateral resolution (pixel size) of about 0.3 µm with a X50 objective, while the tactile profiles are taken at a sampling interval of 0.5 µm by using a 90° conical tip with an apex of about 2.5 µm radius of curvature. Either the lateral resolution/pixel size, the finite size of the tip, or the void pixels are the main reasons why of the difference between number and positions of the "spikes" in the cross-section area profiles.

Concentrating on the spatial frequency spectrum, it can be noticed that dominant wavelength component are in the range from about 100 µm to 200 µm.

Table 2 Waviness parameters of the cross-section area profile, as reconstructed by optical confocal (opt) and stylus (st) instruments

sampling areas	**#1**		**#2**		**#2b**		**#3**		**#4**		**#5**	
finger evaluation length of 5 mm	*opt*	*st*	*opt*	*st*	*opt*	*st*	*opt*	*st*	*opt*	*st*	*opt*	*st*
$W_at\ (Acs)$[µm^2] (λc 0.25 mm)	11.4	14.6	15.6	18.2	10.8	12.9	9.55	12.9	7.88	8.61	13.5	11.1
$Wsk\ (Acs)$ (λc 0.25 mm)	0.02	-0.33	0.36	-0.15	0.17	0.54	-0.04	0.04	0.63	0.15	-0.31	0.40
$Wku\ (Acs)$ (λc 0.25 mm)	2.37	2.36	2.75	2.70	2.61	2.99	2.44	2.62	4.20	2.53	4.41	2.46

Moreover, waviness parameters Wt, Wsk, Wku [6] are calculated using a cutoff of 0.25 µm from the profile of cross-section area variations (Table 2). The total height waviness parameter Wt is here renamed as W_at with the subscript "a", to give evidence of the waviness of the profile of a cross-section area (in µm^2 unit). W_at is the peak parameter, so the larger the W_at the larger is the difference by the maximum and minimum values of the cross-section area. Skewness Wsk relies on the asymmetry while kurtosis Wku on the sharpness of waviness, and are both influenced by the presence of isolated peaks [14].

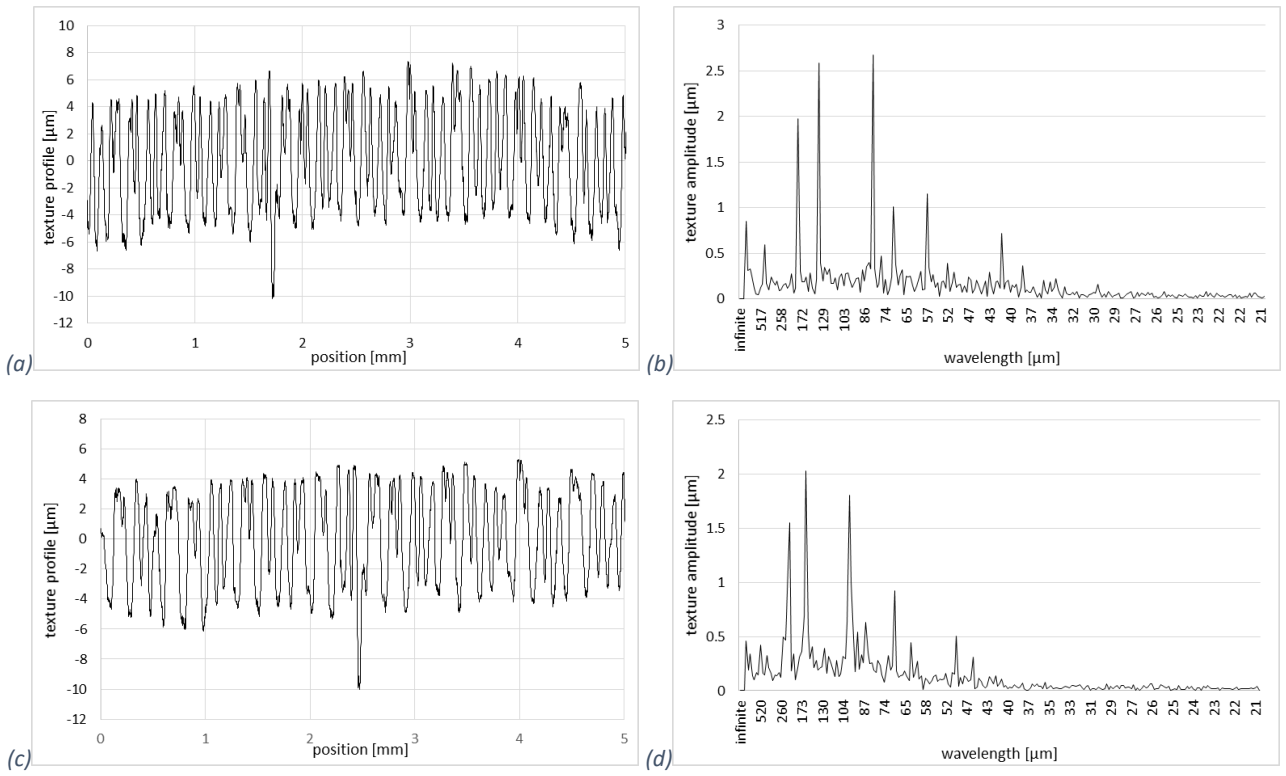

Figure 8 Area #5: Top surface profile and its spatial frequency spectrum obtained by means of (a),(b) optical and (c),(d) stylus profilometers

Furthermore, finger top surface profile calculated by optical confocal and stylus images is compared in Figure 8. These graphs highlight profiles with the same amplitude and frequency of texture, and a more pronounced peak is clearly visible in both profiles. Besides, the dominant wavelengths of the frequency spectrum are in the range from about 100 µm to 200 µm, as in Figure 7. At lower wavelengths (higher frequencies), the stylus profiler is less sensitive due to the finite size of the tactile tip.

Table 3 Roughness parameters (cutoff λc of 1 mm), scaling and fractal dimension of the longitudinal top profile of fingers, as reconstructed by optical confocal (opt) and stylus (st) instruments

sampling areas	**#1**		**#2**		**#2b**		**#3**		**#4**		**#5**	
finger evaluation length of 5 mm	*opt*	*st*	*opt*	*st*	*opt*	*st*	*opt*	*st*	*opt*	*st*	*opt*	*st*
Rz [µm]	17.2	12.4	18.0	17.1	14.4	12.4	14.0	11.2	15.9	7.9	13.1	11.2
Ra [µm]	4.2	3.3	5.2	5.2	3.0	2.7	3.3	2.9	2.1	1.6	3.2	2.9
Rq [µm]	4.8	3.7	5.7	5.7	3.5	3.2	3.8	3.2	2.7	1.9	3.6	3.2
Rq scaling (st. dev.)	0.97 (0.08)	1.06 (0.07)	0.98 (0.09)	1.17 (0.10)	0.90 (0.08)	1.02 (0.07)	0.96 (0.16)	1.08 (0.05)	0.84 (0.07)	0.92 (0.05)	0.91 (0.08)	0.83 (0.19)
fractal dimension (F)	1.00	1.02	1.91	1.04	1.84	1.88	1.03	1.02	1.17	1.13	1.04	1.71
wavelength of the main components of finger profile [µm]	~ (100-200)											

From the top surface profile of fingers as those in Figure 8, roughness parameters are also calculated at all sampled areas, namely the root-mean square Rq, the maximum height Rz and the average Ra (Table 3) [6]. These values show common trends between areas, but with some differences between those from the optical- and stylus-images. Among others, local artefacts of the optical imaging and smoothing effect due to the tactile finite size (lowering Rz) may play a role. Significant differences of top roughness are visible between the various sampling areas, i.e., Rq and Ra have values ranging from about 2 µm to about 6 µm. The estimated relative expanded uncertainty of roughness parameters is of 3 % for Ra and Rq, and of 5 % for Rz.

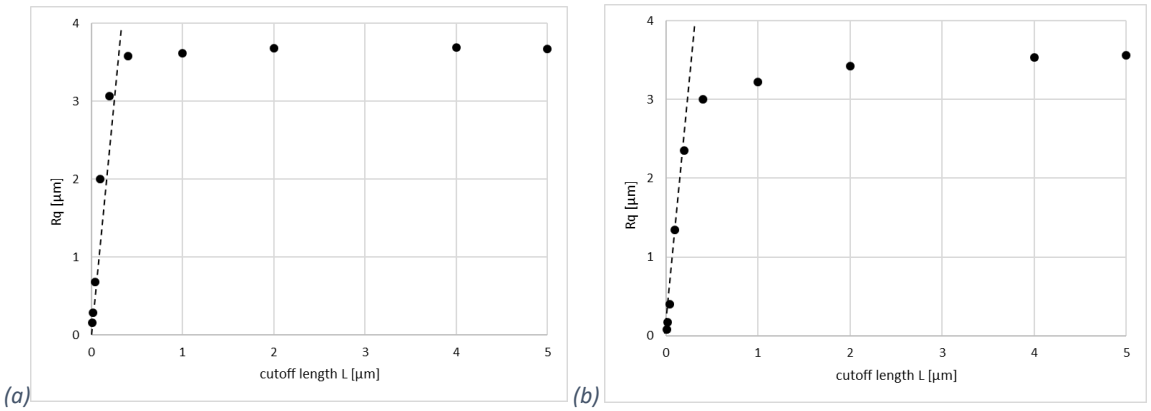

(a) *(b)*

Figure 9 Area #5: Rq top roughness of surface finger at different cutoff lengths. Plots from (a) optical and (b) stylus profiles.

The scaling of the rms roughness is shown in the plots in Figure 9. Rq scales with the cutoff length (L) at the shorter lengths and slightly increase at the longer cutoffs. The slope (dashed lines) of the plot $ln(Rq)$ vs $ln(L)$, is calculated up to 0.4 mm cutoff length for both profiles Rq scaling (α) with values of about 1 and

with a standard deviation of about 0.1 have been obtained by images from optical and stylus profilers at all sampling areas.

Finally, from the top surface profile is also calculated the fractal dimension F, which is a parameter describing the complexity of the surface. As discussed in literature [15], the fractal parameter F relates to the scaling of rms roughness by the relation $\alpha \sim 2 - F$. This relation is mostly confirmed by the values obtained in the analysis of finger roughness both by stylus and optical profilers.

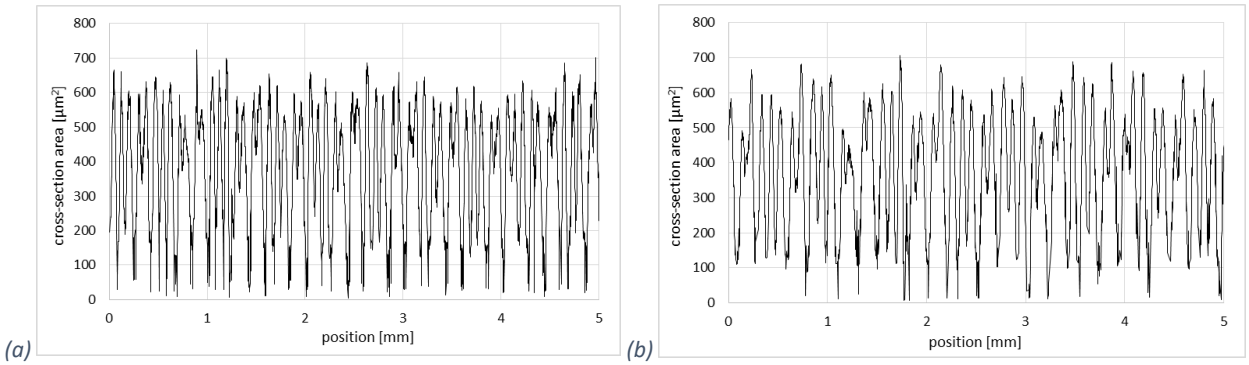

Figure 10 Area #5: Profiles of the cross-section area at position #2, as reconstructed by optical (a) and stylus (b) profilers

It is worth noting that a common trend between parameters calculated from the cross-section area "profile" and those from the top finger profile is present at almost all sampled areas and further support the achieved results. In fact, as can be seen in Table 1, Table 2 and Table 3, all values are similar, except for sampling area #2, which has values larger than those at the other areas. This is due to the fact that this area presents more shrinkages in the cross-section area, with the consequent high value of rms (Acs). Furthermore, the alternation of large and narrow zones leads to high values of the total height waviness parameter $W_a t$, and of the roughness parameters of top finger profile. Consequently, a larger value of standard deviation of residuals by a linear fit of the calculated resistance Rcs is observed at the area #2 (Table 1), with a significant deviation by calculated and measured resistance. Future steps will concern further development of the model of the measured resistance in the presence of large irregularities of the finger morphology.

The fractal dimension, which describes the complexity of a surface as a ratio of the change to the change in scale, relates to the irregularities at the different scales but it is somewhat difficult to get evidence of a common trend by its values and those of the other parameters, either waviness or roughness.

4.2 Resistance measurements

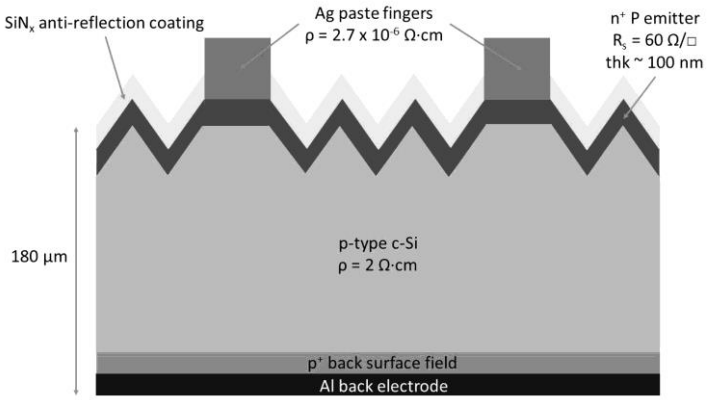

Figure 11 Sketch of the cross-section of a BSF cell (source: refs. [12,16])

As sketched in Figure 11, silver paste of fingers usually come in contact with the phosphorous emitter layer during the rapid thermal processing step, in which silver precipitates epitaxially on silicon. The ohmic contact formation is influenced by the sheet resistance of the emitter layer [17], which is 60 Ω/□ and 100 nm thick [13].

When measuring the resistance of a finger segment, the parallel resistance due to the other fingers has to be taken into account, and in particular the parallel resistance of the finger in pairs. Likewise, the influence of the semiconductor p-type, whose resistivity is $\rho = 2$ Ω·cm, in parallel with the sheet resistance of the emitter is also present.

The resistance R' measured at a given point of the finger segment is described by a linear model reported in the equation (3), assuming equal the resistance of segments of the same length represented in the equivalent circuit given in Figure 12. Looking at the equation (3), R_d is the resistance in serie with the reference and working probes, while R_c is the parallel resistance due to the fingers in parallel with the segment of resistance $R_{ab} = R_a + R_b$, and its value is $R_c \sim \frac{R_{ab}}{3}$ because of the parallel of the three branches. Moreover R_b is the resistance of the finger segment of length L_b from the busbar to the moving probe electrode, and R_a is the resistance of the finger segment of length L_a from the moving electrode to the mid interconnecting section pair. Furthermore, the resistance in a specific point is calculated as the parallel between R' and Res, which is the parallel resistance from the emitter and the base substrate assuming a wafer section of width equal to the finger lateral spacing. Then, the resistance R of a finger segment is given by the difference of the resistances measured with the moving probe at the beginning and at the end of the segment with the reference probe on the busbar (Figure 3). In these way, the contact serie resistance R_d cancels by the difference, but an uncertainty component associated to the contact resistance is included in the budget.

$$R' = R_d + \frac{R_a \cdot (R_b + R_c)}{R_a + R_b + R_c} \qquad (3)$$

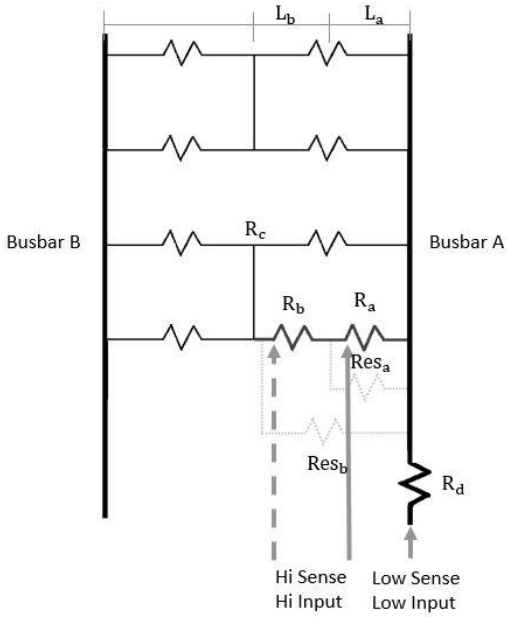

Figure 12 Sketch of the equivalent circuit assumed for continuous fingers

Table 4 shows the measured resistance together with the resistance Rcs computed from the cross-section area. These two independently obtained resistance values of the same segment agree quite well either for optical and stylus images, except for the sampled area #2, which has a larger calculated Rcs value. The larger difference of resistance is observed for a finger having irregularities of topography somewhat larger than those of the other sampled areas, as demonstrated either by the rms (Acs) value of the cross-

section area along the finger segment, or by the standard deviation of the residuals of a linear fit of the calculated resistance Rcs (Table 1). When compared, larger irregularities of topography at the area #2 are also detected by the peak waviness parameter W_at of the cross-section area profile (Table 2), and by the roughness parameters Ra, Rq, Rz (Table 3) of the finger top profile. In presence of significant variations of the finger cross-section area, the model of the resistance measurement does not fully match our assumption of equal resistance of segments of the same length and requires further steps to explain the observed difference. Our study highlights a good consistency of calculated and measured resistance of finger segments showing variations up to $rms\ (Acs)/Acs$ < 0.3 of the cross-section area.

Table 4 Comparison between calculated resistance and measured resistance using optical and stylus profilers

sampling areas	**#1**		**#2**		**#2b**		**#3**		**#4**		**#5**	
finger evaluation length of 5 mm	*opt*	*st*	*opt*	*st*	*opt*	*st*	*opt*	*st*	*opt*	*st*	*opt*	*st*
resistance *R* [mΩ]	434		403		375		371		323		349	
cross-section area based calculated resistance *Rcs* [mΩ]	440	416	637	736	383	401	357	403	347	375	397	403

In order to confirm the model reported in equation (3), one finger of the cell was interrupted at the mid-interconnection of fingers pair, as shown in Figure 13. In this way, the finger is in series with the busbar and there is no more the parallel with the other three branches R_c. The resistance of the finger interrupted R_{int}, described in equation (4), is equal to the difference between the resistances measured in two points, so the term in series due to the contact is not considered. Specifically, Rm_a is the resistance measured in the segment L_a, Rm_b is the analogous resistance referred to the segment L_b, Res_a is the resistance due to the parallel between the emitter and the base substrate (semiconductor) in the zone a, and Res_b is the same but in position b. Note that in the sketch reported in Figure 13 the resistance R_a is given by the parallel between Rm_a and Res_a, and the same holds for R_b.

$$R_{int} = R_b - R_a = \frac{Rm_b \cdot Res_b}{Res_b - Rm_b} - \frac{Rm_a \cdot Res_a}{Res_a - Rm_a} \qquad (4)$$

Note that R_a and Res_b are calculated considering the entire surface of the cell, and not only a small area.

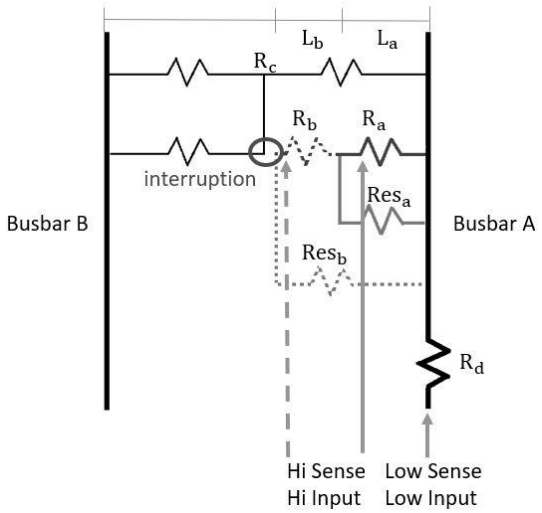

Figure 13 Sketch of the equivalent circuit assumed for interrupted fingers

The resistance measured at increasing length of a finger segment 5 mm long in area #3 is shown in Figure 14. Figure 14 (a) shows a slight second order trend due to the fact that the finger analyzed is in parallel with the other finger pairs and also with the parallel of the emitter-base substrate. Besides, local variations possibly due to probing effects are also visible. The resistance R calculated with equation (3) is 371 mΩ. After interruption of the finger the measured resistance shows the behavior plot in Figure 14 (b), in which a dominant linear trend of resistance value is seen at the increasing of the segment length because the parallel with the other pairs is interrupted. The resistance R_{int} calculated with equation (4) is 376 mΩ.

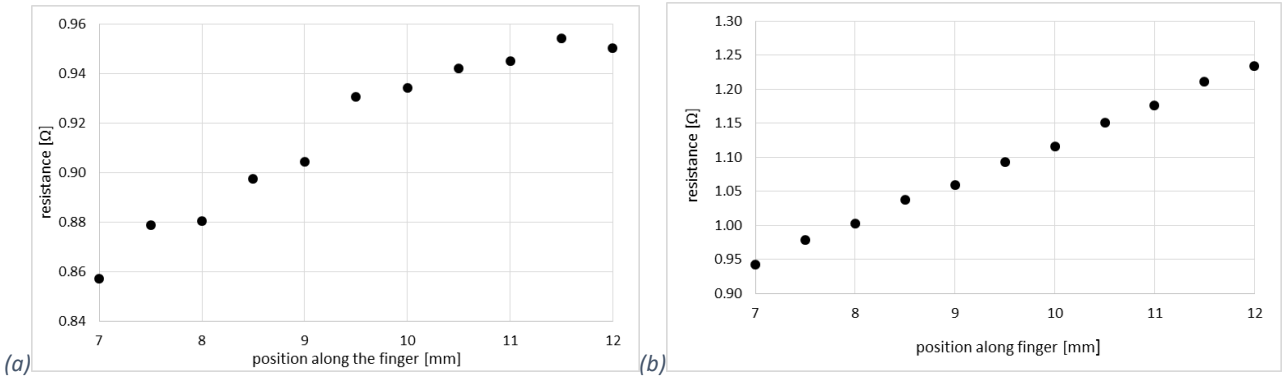

Figure 14 Resistance measurements performed on the sampled area #3 before (a) and after (b) mechanical interruption of the finger. In abscissae are reported the position along the finger of the working electrode respect to the busbar 2.

5. Uncertainty

Morphological and electrical parameters of the fingers are calculated according to the models given above. Main components of the uncertainty are estimated by using the models and are given by their significance level in the Tables 5 and 6, namely for the cross-section area and the calculated resistance of the fingers at the selected areas.

The uncertainty of the cross-section area of fingers reconstructed by 3D confocal optical imaging (Table 5) is estimated by including the repeatability of the reconstruction itself by independent runs and repeated data analysis, the uncertainties of finger sizes (thickness, width, slope) of the assumed trapezoidal cross-section, and of local morphology changes. All these components are estimated by the image analysis using the ISO 5436 tool of SPIP [7]. Other contributions (levelling, filtering) are also included. A relative expanded uncertainty of about 14% is estimated with a finger of 40 µm nominal width, and 15 µm thickness.

Table 5 Uncertainty components of the cross-section area of fingers by 3D confocal optical imaging

source of uncertainty	**significance level**	
	low	***high***
repeatability		✓
thickness		✓
width, slope		✓
morphology local changes		✓
levelling	✓	
relative expanded uncertainty	**~ 14%**	

The uncertainty of the cross-section area-based calculated resistance Rcs (Table 6) takes into account the main components of the uncertainty of the cross-section area as calculated above, and of the uncertainty associated to the assumed resistivity of the silver paste of fingers. A relative expanded uncertainty of about 17 % is estimated for the resistance calculated for a finger segment 5 mm long.

Table 6 Uncertainty components of the cross-section area-based calculated resistance

source of uncertainty	significance level	
	low	***high***
cross-section area		✓
resistivity		✓
segment length	✓	
relative expanded uncertainty	**~ 17%**	

Furthermore, the uncertainty of the resistance R of fingers as measured at given segments takes into account the repeatability itself, the uncertainty of the adopted model (including the influence of parallel fingers) and of the resistance by the emitter layer and by the base substrate semiconductor of the PV cell. A repeatability of about 2 % of the measured resistance is achieved by repeated probe-finger contacts at a given position. A relative expanded uncertainty of about 15 % is estimated for the resistance calculated by the difference of the resistance measured at the ends of a finger segment 5 mm long.

6. Conclusions

Printed linear conductors (fingers) made on a PV cell of standard design have been extensively characterized by morphology- and resistance-based measurements carried out by optical and tactile instruments on several sampling areas evenly distributed along the PV cell. Morphology parameters of the top roughness and mean section area of fingers from 3D surface images reconstructed by stylus and optical instruments are well in agreement. Furthermore, a novel approach is utilized in correlating morphology- and function-related parameters of printed linear conductors. The locally measured resistance directly relates with the resistance calculated by the reconstructed morphology, assuming a given value of finger resistivity. In this way, a good agreement of calculated and measured resistance is achieved with flawless fingers. Besides, a better insight of finger morphology is somewhat given by selected parameters of the top roughness and cross-section variations. The outstanding comparison and/or correlation of parameters may support a further development of custom-design and application-oriented material measures suitable to support traceability of in-line measurements in highly parallel manufacturing (HPM).

Acknowledgments

The parent project MetHPM is delivered under the EMPIR initiative, which is co-funded by the EU's Horizon 2020 research and innovation programme and the EMPIR Participating States.

7. References

[1] C. Khadilkar, S. Sridharan, T. Pham, A. Shaikh, S. Kim, Characterization of front contact in a silicon solar cell, *Technical digest of the International PVSEC-14*, Bangkok, **2004**, 443-4

[2] A. Zekry, G. Heldallal, Effect of MS contact on the electrical behaviour of solar cells, *Solid-State Electronics*, **1988**, 31, 1, 91-97

[3] J. Petzing, M. Jackson, R. Parkin, M. Tailor, P. Phairatt, Real-time surface defect detection and traceable measurement of defect in 3D, *11th International Symposium on Measurement and Quality Control*, Cracow, **2013**

[4] JCGM 200:2012, International vocabulary of metrology – Basic and general concepts and associated terms (VIM), 3rd edition, https://www.bipm.org/utils/common/documents/jcgm/JCGM_200_2012.pdf

[5] R. Leach, C. Giusca, K. Rickens, O. Riemer, P. Rubert, Development of material measures for performance verifying surface topography measuring instruments, *Surf. Topogr.: Metrol. Prop.*, **2014**, 2, 025002
[6] ISO 4287:1997 Geometrical Product Specifications (GPS) -- Surface texture: Profile method -- Terms, definitions and surface texture parameters, https://www.iso.org/standard/10132.html
[7] ISO/DIS 25178-607 Geometrical product specifications (GPS) — Surface texture: Areal — Part 607: Nominal characteristics of non-contact (confocal microscopy) instruments, https://www.iso.org/obp/ui/#iso:std:iso:25178:-607:dis:ed-1:v1:en
[8] T. J. Fellers, M. W. Davidson, Introduction to Confocal Microscopy, Olympus Fluoview Resource Center, http://fluoview.magnet.fsu.edu/theory/confocalintro.html
[9] Image Metrology SPIP, website https://www.imagemet.com/products/spip/
[10] DigitalSurfMountainsMap 7 Premium, website http://www.digitalsurf.com/en/mntpremium.html
[11] NIST Engineering Metrology Toolbox, http://emtoolbox.nist.gov/Main/Main.asp
[12] L. Jiang, W. Zhang, T. Guo, D. Kapp, L. Yan, L. Wang, An improved mathematical modelling to simulate metallization screen pattern trend for silicon solar cell, *Photovoltaic Specialists Conference (PVSC),2013 IEEE 39th*, **2013**, 2641-2645
[13] H. Hannebauer, T. Dullweber, T. Falcon, R. Brendel, Fineline printing options for high efficiencies and low Ag paste consumption, *Energy Procedia*, **2013**, 38, 725-731
[14] D. N. Joanes, C. A. Gill, Comparing measures of sample skewness and kurtosis, *Journal of the Royal Statistical Society: Series D (The Statistician*), **1998**, 47, 183-189
[15] C.-C. Chou, H.-H. Lin, Fractal dimension and surface topography on the diamond deposition of seeded WC–Co substrates, *Journal of Applied Physics*, **2010**, 107 (7), 073510
[16] S. W. Glunz, R. Preu, D. Biro, Crystalline Silicon Solar Cells, in Comprehensive Renewable Energy, Chapter 1.16, **2012**, *Elsevier*, ISBN: 978-0-08-087873-7
[17] Y. Yang, S. Seyedmohammadi, U. Kumar, D. Gnizak, E. Graddy, A. Shaikh, Screen Printable Silver Paste For Silicon Solar Cells With High Sheet Resistance Emitters, *Energy Procedia*, **2011**, 8, 607–613